Simulation of Shor algorithm for discrete logarithm problems with comprehensive pairs of modulo p and order q

Kaito Kishi¹, Junpei Yamaguchi², Tetsuya Izu², and Noboru Kunihiro³

The discrete logarithm problem (DLP) over finite field polynomial-time algorithm on classical computers. However turn computers. Nevertheless, there are only few examples modulo p and order q. In this paper, we constructed such querical and q up to 32 qubits using a quantum simulator with PRIMI success probabilities, which had previously been heuristically of the success probability of Shor's algorithm for solving the Additionally, we generated 1,015 quantum circuits for large compared them for p=2048 bits between safe-prime groups strength of safe-prime groups and Schnorr groups is the sar strength of the latter decreases to the bit length of p in the was experimentally and theoretically shown that when a ripp strength of a Schnorr group with p=2048 bits under Shor with p=1024 bits.

Introduction

Throduction

Throduction

The biffer live of the DLP provise denoted in the polynomial strength of a given element $h \in \langle g \rangle$ is called the Discrete Logarithm The discrete logarithm problem (DLP) over finite fields, commonly used in classical cryptography, has no known polynomial-time algorithm on classical computers. However, Shor has provided its polynomial-time algorithm on quantum computers. Nevertheless, there are only few examples simulating quantum circuits that operate on general pairs of modulo p and order q. In this paper, we constructed such quantum circuits and solved DLPs for all 1,860 possible pairs of pand q up to 32 qubits using a quantum simulator with PRIMEHPC FX700. From this, we obtained and verified values of the success probabilities, which had previously been heuristically analyzed by Ekerå. As a result, the detailed waveform shape of the success probability of Shor's algorithm for solving the DLP, known as a periodic function of order q, was clarified. Additionally, we generated 1,015 quantum circuits for larger pairs of p and q, extrapolated the circuit sizes obtained, and compared them for p = 2048 bits between safe-prime groups and Schnorr groups. While in classical cryptography, the cipher strength of safe-prime groups and Schnorr groups is the same if p is equal, we quantitatively demonstrated how much the strength of the latter decreases to the bit length of p in the former when using Shor's quantum algorithm. In particular, it was experimentally and theoretically shown that when a ripple carry adder is used in the addition circuit, the cryptographic strength of a Schnorr group with p = 2048 bits under Shor's algorithm is almost equivalent to that of a safe-prime group

for a given element $h \in \langle g \rangle$ is called the Discrete Logarithm Problem (DLP). The difficulty of the DLP varies depending On the group, but when G is \mathbb{F}_p^{\times} , which is the multiplicative group of a finite field \mathbb{F}_p of prime order p, no polynomialtime algorithm is known for classical computation. This dif-ficulty is utilized to ensure the security of cryptographic algorithms such as Diffie-Hellman (DH) key exchange [1] and Digital Signature Algorithm (DSA) [2]. The Number Field Sieve (NFS) [3] is a known classical algorithm for solving the ${}^{\circ}$ DLP in the multiplicative group \mathbb{F}_p^{\times} . Experimental results using the NFS have solved DLP instances with modulos pup to 240 digits (795 bits) (See Table 1), and the computational complexity of the NFS is sub-exponential in the size of p, specifically $O(\exp(((64/9)^{1/3} + o(1))(\ln p)^{1/3}(\ln \ln p)^{2/3}))$. Therefore, it is recommended to set p to be at least 2048 bits for DH key exchange and DSA [4]. According to the Pohlig-Hellman algorithm [5], a classical algorithm for solving DLP in general cyclic groups, it is desirable for the order q to be a large prime. In the multiplicative group \mathbb{F}_p^{\times} , q always divides p-1, so when q=(p-1)/2 is prime (i.e., p is a safe-prime), the group has the highest resistance to the Pohlig-Hellman algorithm. In this paper, we refer to pairs (p,q) where pand q are primes and q = (p-1)/2 as safe-prime groups.

For DSA signatures, it is desirable for q to be small because modular arithmetic with the prime q is required. The computational complexity of square root algorithms such as the Baby-step Giant-step method [6], a classical algorithm for solving the DLP in general cyclic groups of order q, is exponential in the size of q, specifically $O(\sqrt{q})$. By comparing the computational time required for the NFS and square root algorithms, it is recommended to set q to 224 or 256 bits when p is 2048 bits, and q to 256 bits when p is 3072 bits [2, 7]. In this paper, we refer to pairs (p,q) that satisfy such relationships as Schnorr groups. Importantly, in classical computation, if p matches and q is at least the qof the Schnorr group, the computational effort required to solve the DLP is the same.

In 1994, Shor proposed a quantum algorithm that can solve the DLP in polynomial-time [8,9]. This algorithm does not tolerate errors in qubits, so it cannot solve large-scale problems on currently developed NISQ (Noisy Intermediate Scale Quantum) computers. However, if an FTQC (Fault-Tolerant Quantum Computer) is realized, there would be a high risk that cryptographic algorithms based on the DLP will be broken.

Shor's quantum algorithm can also solve the factorization problem in polynomial-time, and estimation of the resources required to factor a 2048 bit RSA composite number have been reported [10–12]. In [10], the coset representation of modular integers, windowed arithmetic, and oblivious carry runways are used to minimize the number of Toffoli gates,

¹Quantum Laboratory, Fujitsu Research, Fujitsu Limited, 4-1-1 Kawasaki, Kanagawa 211-8588, Japan ²Data & Security Laboratory, Fujitsu Research, Fujitsu Limited, 4-1-1 Kawasaki, Kanagawa 211-8588,

³Institute of Systems and Information Engineering, University of Tsukuba, 1-1-1 Tennodai, Tsukuba, Ibaraki 305-8573, Japan

and considerations are made for implementation using surface codes that account for the time of the magic state factory. This approach estimates the number of Toffoli gates and the computation time required to factorize a 2048 bit RSA composite number. Similarly, [11] estimates the factorization time using fewer qubits, although with increased time compared to [10], by using 3D color codes and quantum memory. Nevertheless, this resource estimate is highly dependent on the configuration of the actual quantum machine, and particularly the implementation of non-Clifford gates has been significantly improved by methods such as STAR [13–15], zero-level distillation [16], and magic state cultivation [17]. On the other hand, a bottom-up approach involves constructing quantum circuits that can be practically executed on simulators and extrapolating from the obtained gate counts to estimate the gate count for a 2048 bit composite number [12, 18].

There is less analysis on the estimation of solving the DLP using Shor's algorithm compared to the factorization. In the aforementioned [10], the computation time for DLP is estimated for both safe-prime groups and Schnorr groups. It shows that the latter can be solved in a shorter time than the former using Shor's algorithm [8], Ekerå's algorithm [19], and Ekerå-Håstad's algorithm [20]. Furthermore, [21] theoretically demonstrates that $\Omega(\log q)$ depth of group operation queries is required for solving the DLP. However, it remains unclear how p and q specifically affect the time complexity when including the most time-consuming part of Shor's algorithm, the modular exponentiation. Although heuristic theoretical analysis of the success probability has been conducted by Ekerå [22], it needs to be verified whether this holds true when Shor's quantum algorithm is executed precisely. As for implementation examples, there are experiments on simulators using Qiskit [23] and on actual quantum computers [24]. The former plots the number of gates and success probability, but does not consider how these depend on the pair of p and q. For the latter, only the experiment solving $2^x \equiv 1 \pmod{3}$ (p=3, q=2) has been successful, making it difficult to analyze for larger values. Especially as quantum computers approach FTQC, Shor's algorithm will likely be executed for larger p and q, so it is necessary to gather specific computational examples around this in advance. On the other hand, there is research extending Regev's multidimensional version of Shor's algorithm [25] to the DLP [26], but this will not be addressed here as it increases the number of qubits, making quantum simulation difficult despite the reduction in gate count.

In this study, we comprehensively simulated the quantum circuits of Shor's algorithm for solving the DLP. We solved DLPs on a quantum simulator for all 1,860 pairs of p and q possible up to 32 qubits using the Q-ADD [27] adder circuit, and obtained the actual success probabilities. From this, we compared the distribution of success probabilities and the changes due to the size of the order q with Ekerå's heuristic analysis [22]. Additionally, we selected 1,015 pairs of larger p and q, and obtained the number of gates and depth of the quantum circuits before and after optimization using the R-ADD [28] adder circuit. Using these results, we extrapolated the circuit scale for 2048 bit as in [12,18] in a bottom-up manner. In this way, we specifically demonstrated how the

cipher strength of the Schnorr group, which is equivalent to the safe-prime group in classical computation, decreases to the strength of a safe-prime group with a smaller p under quantum computation.

In this paper, we use the following notations. For a natural number x > 0, the logarithm to the base 2 is denoted by $\log x$, and the natural logarithm is denoted by $\ln x$. For a non-negative integer x, its size (bit length) is denoted by |x|, and the function that rounds x to the nearest integer is denoted by |x|.

2 Shor's Algorithm for the DLP

Shor's algorithm for solving the DLP can be divided into two main stages:

- 1. The quantum computation part, which involves the calculation of modular exponentiation, the inverse quantum Fourier transform, and measurement.
- 2. The classical computation part, which uses the measurement results to obtain s.

Each step will be described in sequence.

2.1 The quantum computation part

A set of qubits is divided into three registers, with the number of qubits in each register denoted as $v_1, v_2, w \in \mathbb{N}$, and the following state is prepared using the Hadamard gate:

$$\frac{1}{\sqrt{2^{v_1+v_2}}} \sum_{x_1=0}^{2^{v_1}-1} \sum_{x_2=0}^{2^{v_2}-1} |x_1\rangle |x_2\rangle |0^w\rangle.$$
 (1)

Next, the X gate is applied to the least significant bit of the third register:

$$\frac{1}{\sqrt{2^{v_1+v_2}}} \sum_{x_1=0}^{2^{v_1}-1} \sum_{x_2=0}^{2^{v_2}-1} |x_1\rangle |x_2\rangle |0\cdots 01\rangle.$$
 (2)

Then, the modular exponentiation $h^{x_1}g^{x_2} \mod p$ is computed and stored in the third register. The specific method for this computation is described in the later section Construction of Quantum Cirtuit. The result of this computation is as follows:

$$\frac{1}{\sqrt{2^{v_1+v_2}}} \sum_{x_1=0}^{2^{v_1}-1} \sum_{x_2=0}^{2^{v_2}-1} |x_1\rangle |x_2\rangle |h^{x_1}g^{x_2} \bmod p\rangle.$$
 (3)

This is equivalent to the following [38]:

$$\frac{1}{\sqrt{2^{v_1+v_2}q}} \sum_{l=0}^{q-1} \sum_{x_1=0}^{2^{v_1}-1} \sum_{x_2=0}^{2^{v_2}-1} e^{2\pi i(slx_1+lx_2)/q}
\cdot |x_1\rangle |x_2\rangle |\hat{f}(sl,l)\rangle \tag{4}$$

$$= \frac{1}{\sqrt{2^{v_1+v_2}q}} \sum_{l=0}^{q-1} \left(\sum_{x_1=0}^{2^{v_1}-1} e^{2\pi i x_1(sl/q)} |x_1\rangle \right)
\cdot \left(\sum_{x_2=0}^{2^{v_2}-1} e^{2\pi i x_2(l/q)} |x_2\rangle \right) |\hat{f}(sl,l)\rangle \tag{5}$$

Table 1: The progress of solving records for the DLP in the multiplicative group of a finite field \mathbb{F}_p^{\times} . A strong-prime refers to a large prime number p for which the largest prime factors of both p-1 and p+1 are also large; for more details, see [29].

Date solved	Modulo	Solver	Remarks
June 18, 2005	130 digits	Joux, Lercier [30]	strong-prime
December 22, 2006	135 digits	Dorofeev, Dygin, Matyukhin [31]	strong-prime
February 5, 2007	160 digits	Kleinjung [32]	safe-prime
June 11, 2014	180 digits	Bouvier, Gaudry, Imbert et al. [33]	safe-prime
June 16, 2016	232 digits	Kleinjung, Diem, Lenstra et al. [34]	safe-prime
February 2, 2019	240 digits	Boudot et al. [35–37]	safe-prime

where $|\hat{f}(l_1, l_2)\rangle = \frac{1}{\sqrt{q}} \sum_{j=0}^{q-1} e^{-2\pi i l_2 j/q} |g^j \mod p\rangle$. Applying the inverse quantum Fourier transform results in the following:

$$\frac{1}{\sqrt{q}} \sum_{l=0}^{q-1} |\widetilde{sl/q}\rangle |\widetilde{l/q}\rangle |\widehat{f}(sl,l)\rangle. \tag{6}$$

Here, $\widetilde{sl/q}$ in the first register is the v_1 -bit approximation of β/q in

$$sl/q = \alpha + \beta/q \quad (\alpha, \beta \in \mathbb{Z}, 0 < \beta < q)$$
 (7)

and l/q in the second register is the v_2 -bit approximation of l/q. Measuring the first and second registers concludes the quantum computation part. The procedure up to this point is described by the quantum circuit shown in Figure 1.

In [22], it is stated that the qubits of the first and second registers can be recycled using the semi-classical quantum Fourier transform with a uniform superposition. Since the quantum circuit is not shown, it is explicitly illustrated here as Figure 2.

While the existing method in Figure 2 can minimize the number of qubits in the control register to one, increasing it to two as in Figure 3 allows the parts enclosed by the dashed lines to be executed simultaneously, reducing the time depth of the quantum circuit. The optimality of this is proved in the Appendix. Additionally, a faster method is shown in the Appendix for cases where the measurement time to obtain $m_0, \ldots, m'_0, \ldots$ is longer than each part of modular exponentiation. In the implementation on the quantum simulator [39, 40] used in this study, these methods utilizing the semi-classical inverse quantum Fourier transform were not employed due to the constraints of the simulator. However, in actual quantum computer implementations, these methods can be applied not only to the DLP but also to Shor's algorithm for integer factorization in general.

2.2 The classical computation part

The purpose of this part is to determine s from the $\widetilde{sl/q}$ and $\widetilde{l/q}$ obtained in the quantum computation part. First, we determine $l \in \mathbb{Z}$ from $\widetilde{l/q}$. If $2^{v_2} > q$, l can be obtained by $l = \lceil \widetilde{l/q} \cdot q \rfloor$. Similarly, if $2^{v_1} > q$, β can be determined from $\beta = \lceil \widetilde{sl/q} \cdot q \rfloor$.

Since l and β have been determined up to this point, combining them with s and α , the following indeterminate

equation is obtained from (7):

$$ls - q\alpha = \beta. (8)$$

Here, since q is a prime number and known, taking both sides modulo q gives:

$$ls = \beta \pmod{q} \tag{9}$$

$$s = \frac{\beta}{l} \pmod{q}. \tag{10}$$

Thus, s can be determined.

In previous research, continued fraction expansion was used [22], but this rounding method allows for a slightly faster determination.

2.3 Space and Time Complexity

Regarding the space complexity represented by the number of qubits, the number of qubits in the first and second registers, derived from the process of determining l and β in the classical computation part, is given by

$$v_1 = v_2 = |\log q| + 1. \tag{11}$$

This result is significantly different from the case of factorization. In Shor's algorithm for factoring a composite number N, the order q, which is the denominator of the value held by the first register after the inverse quantum Fourier transform, is unknown. Therefore, to accurately estimate the true rational number from the measurement result, the first register requires $2\lceil \log N \rceil + 1$ qubits, and the continued fraction expansion algorithm must be executed from there [38]. Consequently, in the case of the DLP, the number of qubits required for the first and second registers is given by (11), and the estimation uses rounding and an indeterminate equation after multiplying by q instead of continued fraction expansion, which is different from factorization. Note that there is a method to add extra qubits to the first register to achieve a success probability of over 99% [22], but this consideration is omitted here due to the exponential load increase on classical computers running quantum simulators as the number of qubits increases.

The third register only needs to store values less than p, so the number of qubits required is

$$w = \lceil \log p \rceil. \tag{12}$$

Additionally, let A_{space} be the auxiliary qubits for modular exponentiation. This varies depending on the addition

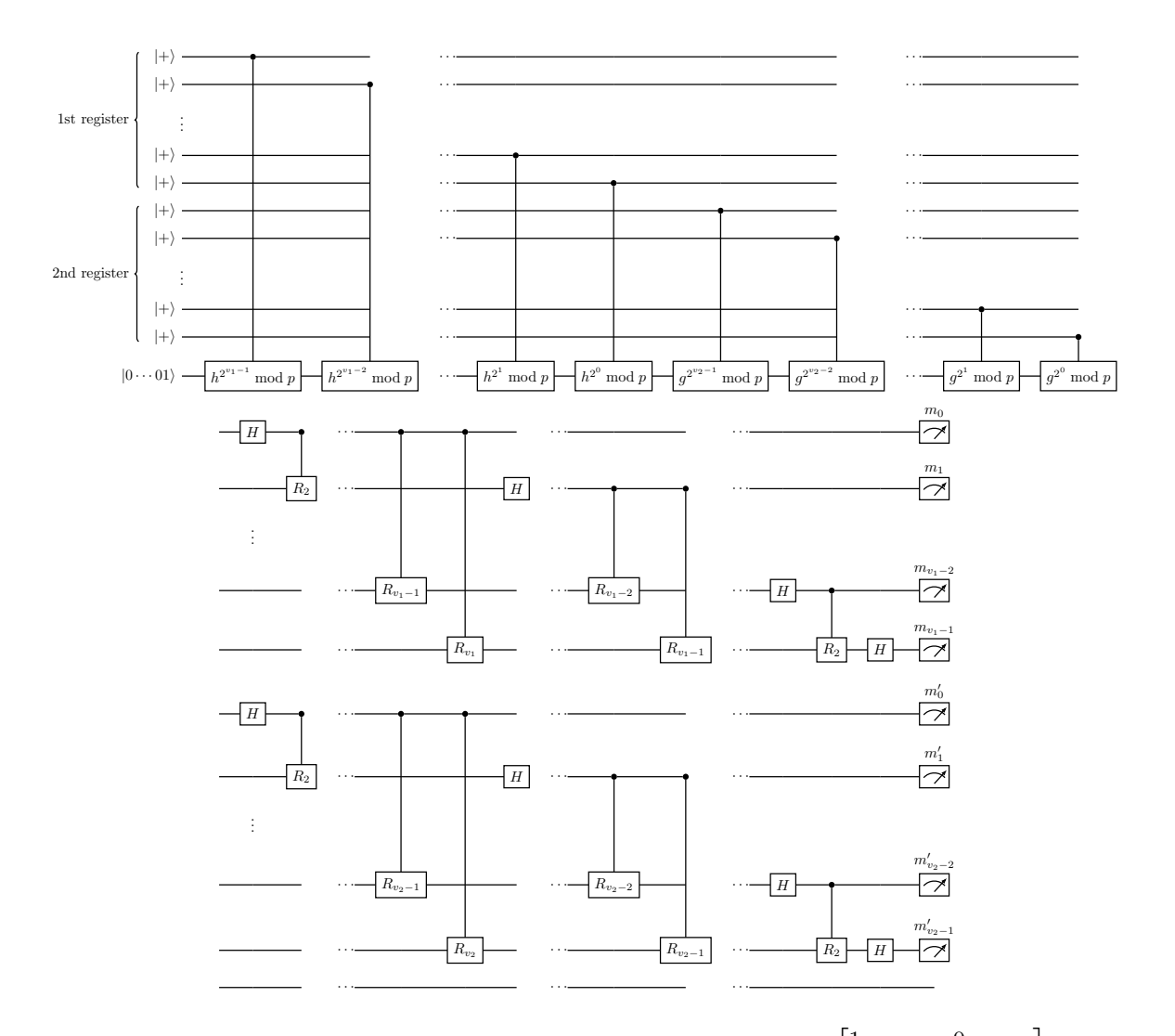


Figure 1: Quantum circuit for solving the DLP using Shor's algorithm. Let $R_j = \begin{bmatrix} 1 & 0 \\ 0 & \exp(-2\pi i/2^j) \end{bmatrix}$. The first part of the circuit on the top is for modular exponentiation, and the second part of the circuit on the bottom is for the inverse quantum Fourier transform.

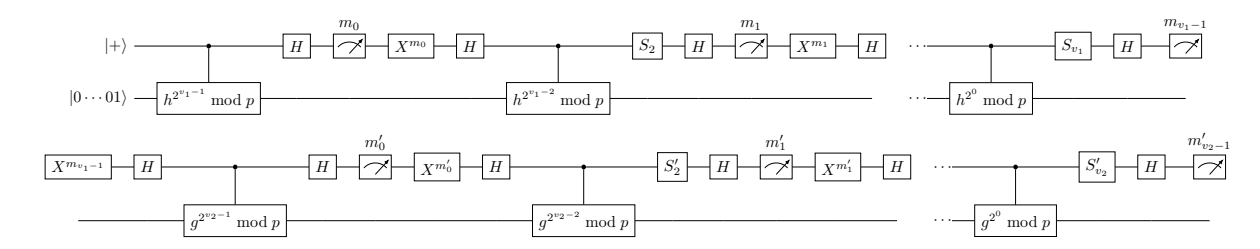


Figure 2: Quantum circuit for solving the DLP using Shor's algorithm when the number of qubits in the control registers is set to 1 by employing the semi-classical inverse quantum Fourier transform. Let $S_j = \begin{bmatrix} 1 & 0 \\ 0 & \exp(-2\pi i \sum_{l=2}^j m_{j-l}/2^l) \end{bmatrix}$ and $S_j' = \begin{bmatrix} 1 & 0 \\ 0 & \exp(-2\pi i \sum_{l=2}^j m_{j-l}'/2^l) \end{bmatrix}.$

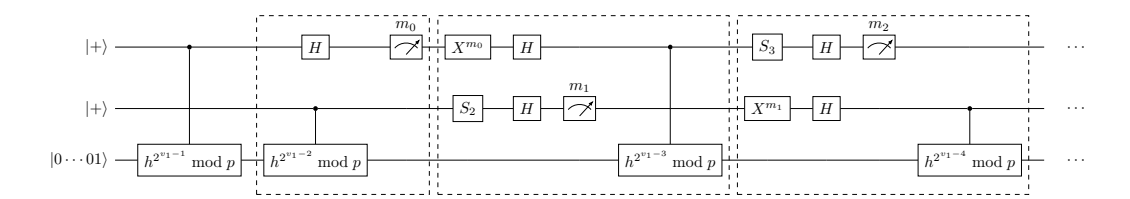


Figure 3: Quantum circuit for solving the DLP using Shor's algorithm when the number of qubits in the control registers is set to 2 by employing the semi-classical inverse quantum Fourier transform and reducing the time depth of the quantum circuit. The parts enclosed by dashed lines can be executed in parallel.

method adopted in modular exponentiation, and the specific form will be discussed in the next section. Therefore, the space complexity is

$$v_1 + v_2 + w + A_{\text{space}} = \lceil \log p \rceil + 2 \lfloor \log q \rfloor + 2 + A_{\text{space}}.$$
(13)

However, as shown in the Quantum Computation Part, if the semi-classical inverse quantum Fourier transform is used, the first and second registers can be combined into 1 or 2 qubits, so

$$1 + w + A_{\text{space}} = \lceil \log p \rceil + 1 + A_{\text{space}} \tag{14}$$

or

$$2 + w + A_{\text{space}} = \lceil \log p \rceil + 2 + A_{\text{space}}. \tag{15}$$

Next, we describe the time complexity represented by the number of gates. The modular exponentiation is executed with the first and second registers as control. In factorization, the time complexity of modular exponentiation is expressed in polynomial order of the bit length of the value to be factored by any known method [41]. From this, similarly in the DLP, when the time complexity of modular exponentiation is expressed as A_{time} , it can be written as $A_{\text{time}} = O(\lceil \log p \rceil^m \lfloor \log q \rfloor^n)$. As with space complexity, the values of m and n for each addition method will be discussed in the next section. Since the time complexity of modular exponentiation is the most dominant in the entire algorithm regardless of the addition method used [10,41], the overall time complexity is

$$A_{\text{time}} = O(\lceil \log p \rceil^m |\log q |^n). \tag{16}$$

3 Construction of Quantum Circuit

Among the quantum circuits of Shor's algorithm, the modular exponentiation, which is the most computationally intensive process, is realized by the Mod-EXP circuit [41]. The number of required qubits and gates varies depending on the implementation method of the adder. There are three types of adder implementations: Q-ADD, GT-ADD, and R-ADD. Q-ADD and GT-ADD require fewer qubits but result in an increased number of gates, whereas R-ADD requires more qubits but fewer gates [41]. On a quantum simulator, as the number of qubits increased, the required memory grows exponentially, making execution difficult. Therefore,

for creating quantum circuits to run on a quantum simulator, Q-ADD was used. For resource estimation at the 2048 bit scale, R-ADD, which can reduce the number of gates and shorten execution time, was used.

Regardless of whether the circuit is based on Q-ADD or R-ADD, as in [12,18,41], Mod-EXP consists of Mod-MUL, Mod-PS, Mod-ADD, and ADD:

- Mod-EXP(a): $|x\rangle |1\rangle \rightarrow |x\rangle |a^x \mod p\rangle$
- Mod-MUL(d): $|y\rangle \to |dy \mod p\rangle$
- Mod-PS(d): $|y\rangle |t\rangle \rightarrow |y\rangle |t + dy \mod p\rangle$
- Mod-ADD(d): $|y\rangle \to |y+d \mod p\rangle$
- ADD(d): $|y\rangle \rightarrow |y+d\rangle$

Here, we construct quantum circuits for DLP rather than for factorization, but the construction method itself is mostly common. However, unlike factorization, there are two variables, p and q, so we will explain how $A_{\rm space}$ and $A_{\rm time}$ introduced in the previous section are described for both Q-ADD based circuits and R-ADD based circuits.

3.1 Q-Add Based Circuits

Q-ADD is a method that uses quantum Fourier transform as an adder [27,42]. The construction method for modular exponentiation circuits using Q-ADD is the same as in [12, 18]. Therefore, when implementing Mod-ADD, additional bits for the range of the complement of the modulo p and an extra bit are required (see Figure 5 in [27] for details), resulting in

$$A_{\text{space}} = (\lceil \log p \rceil + 1) + 1 = \lceil \log p \rceil + 2.$$
 (17)

Regarding time complexity, as in [12, 18, 27], it takes $O(\lceil \log p \rceil^3)$ to execute Mod-MUL once within the range of the modulo p, and since the number of executions is $v_1 + v_2 = 2\lceil \log q \rceil + 2 = O(\lceil \log q \rceil)$, the overall time complexity is given by (16) as

$$O(\lceil \log p \rceil^3 |\log q|). \tag{18}$$

3.2 R-Add Based Circuits

R-ADD is a ripple carry adder [28]. Previous studies estimating the resources of Shor's algorithm on surface codes also based their addition method on this [10]. As in Q-ADD,

the construction method of the modular exponentiation circuit using R-ADD is similar to [12, 18, 41], and in addition to the number of qubits required for Q-ADD, $\lceil \log p \rceil$ qubits are needed, resulting in

$$A_{\text{space}} = (\lceil \log p \rceil + 2) + \lceil \log p \rceil = 2\lceil \log p \rceil + 2. \tag{19}$$

While there are differences in the part related to the number of gates compared to factorization, but they do not affect the order of time complexity, so they are described in the Appendix. Thus, as in [12, 18, 41], it takes $O(\lceil \log p \rceil^2)$ to execute Mod-MUL once in the range of modulo p, and since this is done $v_1 + v_2 = O(\lceil \log q \rceil)$ times, the overall time complexity is

$$O(\lceil \log p \rceil^2 \lfloor \log q \rfloor).$$
 (20)

4 Simulating Quantum Circuits

The results of executing Shor's algorithm for solving the DLP on a quantum simulator are presented. When executing the generated circuits, we utilized Q-ADD, which requires fewer qubits as previously mentioned, and employed mpiQulacs 1.3.1 [40], a state vector simulator developed by Fujitsu. We used a PRIMEHPC FX700 with one node for up to 28 qubits, four nodes for 29-32 qubits, and up to 256 nodes for 36 qubits. Additionally, after generating the quantum circuits, we applied optimize_light from mpiQulacs as an optimization step. This optimization not only includes the greedy method from Qulacs [39] but also reduces interprocess communication by fused-swap gates [40].

On the other hand, for circuit generation aimed at resource estimation, we utilized R-ADD, which requires fewer gates. For optimization, we used the standard optimize_light from Qulacs [39].

4.1 Running Generated Circuits

We executed quantum circuit simulations using Q-ADD for all 1,860 combinations of prime numbers p and q that satisfy

$$q|(p-1) \tag{21}$$

up to 32 qubits. The complete list of these combinations is shown in Table 2. The simulation results confirmed that the correct solution s was obtained for all combinations.

Additionally, as an experiment with large numbers, we solved the DLP of a safe-prime group with (p,q) = (263,131), (347,173), (359,179), (383,191), (467,233), (479,239), (503,251), which can be represented with 36 qubits, using a quantum simulator. Here, p is 9 bits and q is 8 bits. On the other hand, for the Schnorr group, if p and q are chosen such that the time complexity of the NFS and the Baby-step Giant-step methods match, p becomes less than q at the scale of 36 qubits, causing a breakdown. Therefore, the Schnorr group was not used in this experiment. As a result, the correct solution s was obtained, and the time to simulate the optimized quantum circuit until 10,000 samples were obtained ranged from 30 to 103 minutes.

For each combination of p and q, 10,000 samples were experimented, and the success probability of correctly obtaining the solution s from the measurement results was calculated according to the procedures of the Classical Computation Part. Each result is shown in Figure 12, and the change in success probability with q as the horizontal axis is shown as a box plot in Figure 4.

First, let's focus on the minimum and maximum values of the success probability. The minimum success probability was 0.4181, confirmed at q = 3, and the maximum was 0.9133, confirmed at q = 13. There are 505 combinations of p paired with q = 3, and 161 of them had the minimum success probability, so $161/505 \approx 31.9\%$ correspond to this. On the other hand, the maximum value was constituted by only p = 1483. There is another pair with q = 13 that has a success probability exceeding 90%, which is p = 1327 with a success probability of 0.9124. Such minimum and maximum values have not been found in previous theory [22] or simulations [23]. This is thanks to the experiment conducted with all combinations of not only p but also q. The maximum value appears as an outlier in Figure 4, but no outliers appear for $q \geq 19$. This does not necessarily indicate the absence of outliers for such q, but it may be due to the constraint on the number of qubits that can be simulated, limiting the size of p and reducing the number of samples.

Next, let's focus on the behavior of the average success probability. As shown in Figure 4, unlike p in Figure 5, the success probability changes periodically as q increases, with a range of approximately 60% to 80%. Specifically, the success probability reaches a local minimum value just before q is a power of 2 (q = 13, 31, 61) and then immediately reaches a local maximum value. Ekerå's heuristic theoretical analysis [22] shows that the success probability changes periodically with q, and that the success probability is approximately 60% as a local minimum value at values of q that are one less than powers of 2, and approximately 82% as a local maximum value at values of q that are one more than powers of 2. This experimental results confirm that heuristic theoretical analysis. Furthermore, we were able to depict a waveform with an asymmetric shape for q, where the value decreases gradually from the local maximum value and then drops sharply as it approaches the local minimum value. Note that Theorem 3 in [22] shows that when certain conditions listed there including classical post-processing are met, the success probability asymptotically approaches 1 as q approaches infinity. This time, since these conditions are not met and it is under the most naive conditions, no significant change in the probability range was observed, except for a slight upward trend in the maximum value within the initial experimental range of q.

4.2 Resource Estimation by Generated Circuits

We estimate the resources using quantum circuits with R-ADD, which can reduce the number of gates. In [12, 18], ten composite numbers were randomly selected for each bit length of the values to be factored, and quantum circuits were generated to solve them to obtain resource values. The bit lengths of the composite numbers ranged from 8 to 24,

Table 2: All 1,860 possible combinations of p and q up to 32 qubits. Each row represents the number of values q within the minimum and maximum range of the target p. For example, the number of combinations of p and q where q=5 and $p \in [300,600]$ is 10. Additionally, – indicates combinations of p and q that cannot be represented within 32 qubits. The #same-prime group represents the number of combinations of p and q that fall into the same-prime group within the range of p in that row.

P 111 01	100 101	٠.																					
	p											#q										#safe-prime	total
min	max	2	3	5	7	11	13	17	19	23	29	31	37	41	43	47	53	61	83	89	113	group	
0	300	62	28	15	9	4	4	3	2	3	2	0	2	1	1	1	1	0	1	1	1	11	141
300	600	47	22	10	7	5	5	3	3	2	2	2	0	0	1	0	0	1	-	-	-	0	251
600	900	45	24	11	9	6	2	2	2	2	0	1	-	_	-	-	-	_	-	-	-	0	355
900	1200	42	20	12	7	4	4	3	0	2	1	0	-	_	-	-	-	_	-	-	-	0	450
1200	1500	43	21	10	6	4	5	-	_	_	_	-	-	_	-	-	-	_	-	-	-	0	539
1500	1800	39	22	7	5	2	1	-	_	_	_	-	-	_	-	-	-	_	-	-	-	0	615
1800	2100	39	17	10	5	2	5	-	_	_	_	-	-	_	-	-	-	_	-	-	-	0	693
2100	2400	40	21	12	8	-	-	-	_	_	_	-	-	_	-	-	-	_	-	-	-	0	774
2400	2700	36	16	8	8	-	-	-	_	_	_	-	-	_	-	-	-	_	-	-	-	0	842
2700	3000	37	16	8	6	-	-	-	_	_	_	-	-	_	-	-	-	_	-	-	-	0	909
3000	3300	33	18	10	5	-	-	-	-	-	-	-	-	-	-	-	-	-	-	-	-	0	975
3300	3600	40	22	11	7	-	-	-	-	-	-	-	-	-	-	-	-	-	-	-	-	0	1055
3600	3900	36	19	8	6	-	-	-	-	-	-	-	-	-	-	-	-	-	-	-	-	0	1124
3900	4200	35	17	6	2	-	-	-	-	-	-	-	-	-	-	-	-	-	-	-	-	0	1184
4200	4500	36	15	-	_	-	-	-	-	-	-	-	-	-	-	-	-	-	-	-	-	0	1235
4500	4800	36	19	-	_	-	-	-	-	-	-	-	-	-	-	-	-	-	-	-	-	0	1290
4800	5100	35	17	-	_	-	-	-	-	-	-	-	-	-	-	-	-	-	-	-	-	0	1342
5100	5400	31	13	-	_	-	-	-	-	-	-	-	-	-	-	-	-	-	-	-	-	0	1386
5400	5700	38	22	-	_	-	-	-	-	-	-	-	-	-	-	-	-	-	-	-	-	0	1446
5700	6000	33	15	-	_	-	-	-	-	-	-	-	-	-	-	-	-	-	-	-	-	0	1494
6000	6300	36	18	-	_	-	-	-	-	-	-	-	-	-	-	-	-	-	-	-	-	0	1548
6300	6600	34	18	-	_	-	-	-	-	-	-	-	-	-	-	-	-	-	-	-	-	0	1600
6600	6900	34	18	-	-	-	-	-	-	-	-	-	-	-	-	-	-	-	-	-	-	0	1652
6900	7200	32	13	-	_	-	-	-	_	-	_	-	-	_	-	-	-	_	-	-	-	0	1697
7200	7500	31	17	-	_	-	-	-	-	-	-	-	-	-	-	-	-	-	-	-	-	0	1745
7500	7800	37	19	-	_	-	-	-	-	-	-	-	-	-	-	-	-	-	-	-	_	0	1801
7800	8100	31	13	-	_	-	-	-	-	-	-	-	-	-	-	-	-	-	-	-	-	0	1845
8100	8400	10	5	-	_	-	-	-	-	-	-	-	-	-	-	-	-	-	-	-	-	0	1860

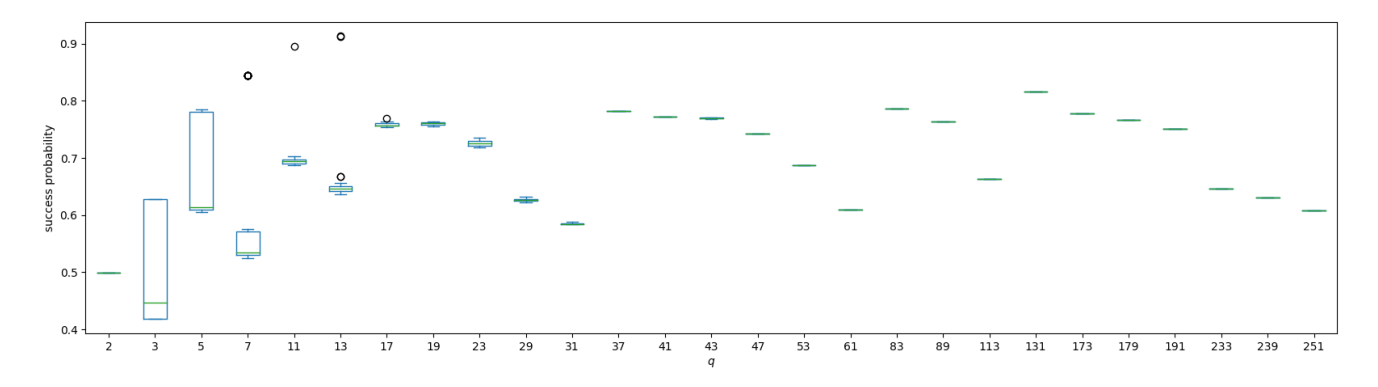


Figure 4: Box plot showing the change in success probability with the size of q.

resulting in a total of 170 composite numbers used in the experiments. On the other hand, in the DLP, there are degrees of freedom not only in the modulo p but also in the order q. Therefore, for each bit length of p and q that can be represented by the given number of qubits, five specific values of p and q were randomly selected, and quantum circuits were generated and experimented with. For example, when the number of qubits is 41, the combinations of bit lengths of p and q that can be represented are $(\lceil \log p \rceil, \lceil \log q \rceil) = (9, 5), (11, 2)$ according to (19) and (13). Among them, only (p,q) = (283,47), (367,61), (431,43)exist for the former, so all three combinations were used. For the latter, more than five combinations exist, so (p,q) = (1871,5), (1901,5), (1321,5), (1597,7), (1231,5)were randomly selected. The number of qubits ranged from 12 to 90, resulting in a total of 1,015 combinations of p and q used in the experiments.

First, the number of qubits matches the surface depicted by the continuous form of the equation obtained by substituting (19) into (13)

$$3\log p + 2\log q + 4\tag{22}$$

(see Figure 6). On the other hand, the depth before and after optimization and the number of non-Clifford gates before and after optimization were fitted using the equation based on (20)

$$a(\log p)^2 \log q + b(\log p)^2 + c \log p \log q + d \log p + e \log q + f$$
(23)

and optimized for $a,b,c,d,e,f\in\mathbb{R}$ using the nonlinear least squares method (curve_fit) of SciPy 1.10.1 [43]. To evaluate the accuracy of this fitting, 10-fold cross-validation was performed, and the average value and mean squared error of the test data for each fold were averaged across all folds, as shown in Table 3. As shown, the errors are within about one-tenth of the average value. From here, regardless of whether optimization is applied or not, the number of gates, circuit depth, and the number of non-Clifford gates can all be expressed by (23), with the differences being only in the coefficients.

The fitting results using all 1,015 combinations as training data are shown in Figures 7, 8, and 9. The parameters are as shown in the Table 4.

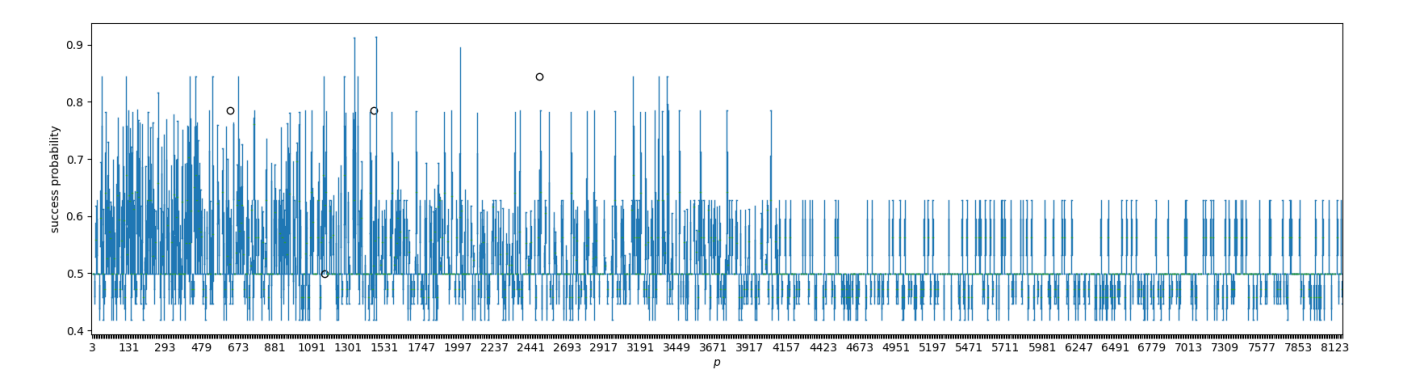


Figure 5: Box plot showing the change in success probability with the size of p.

Table 3: The table shows the average of the test data and the root mean squared error (RMSE) from the test data averaged over all folds, obtained by performing fitting using (23) on each training dataset in the 10-fold cross-validation.

	Average	RMSE
#gates before optimization	7.66×10^{6}	4.22×10^5
#gates after optimization	2.49×10^6	1.36×10^5
depth before optimization	4.20×10^6	2.25×10^5
depth after optimization	1.89×10^{6}	1.00×10^{5}
#non-Clifford gates before optimization	3.56×10^6	1.95×10^5
#non-Clifford gates after optimization	2.38×10^{6}	1.31×10^5

Based on these results, we estimated the resources when p is 2048 bits. When p is 2048 bits, the bit length of q differs between safe-prime groups and Schnorr groups. In safe-prime groups, q is approximately 2047 bits to satisfy p=2q+1. On the other hand, in Schnorr groups, q is 256 bits [44] to match the time complexity of the NFS, which is determined by p, and the Baby-step Giant-step method, which is determined by q. As shown in Table 5, the required number of gates and depth differ between safe-prime groups and Schnorr groups. In classical computation, as is evident from the way p and q are determined in Schnorr groups, the time complexity required to solve the DLP for both, where q is 256 bits or more, is the same. However, this is not the case in quantum computation because the overall time complexity depends on both p and q, as shown in (16).

The strength of Schnorr groups under quantum computation can be measured by the size of p in safe-prime groups. Specifically, when using Shor's quantum algorithm, we investigated the size of p in safe-prime groups that matches the computational complexity of the Schnorr group with p=2048 bits. In (23), for safe-prime groups, since

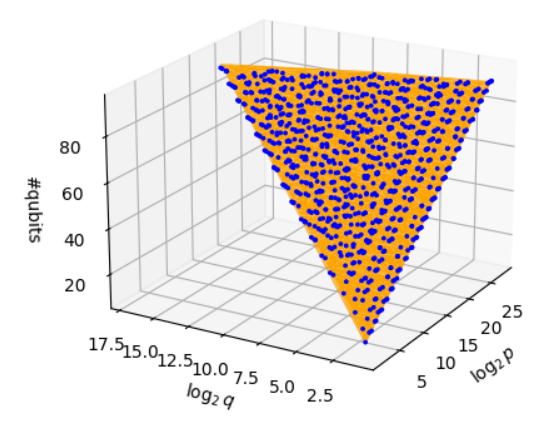


Figure 6: Number of qubits. The blue dots represent the results obtained from each experiment, and the orange surface represents (22).

 $\log q = \log p - 1$, it can be transformed as follows:

$$a(\log p)^{2}(\log p - 1) + b(\log p)^{2} + c\log p(\log p - 1) + d\log p + e(\log p - 1) + f$$

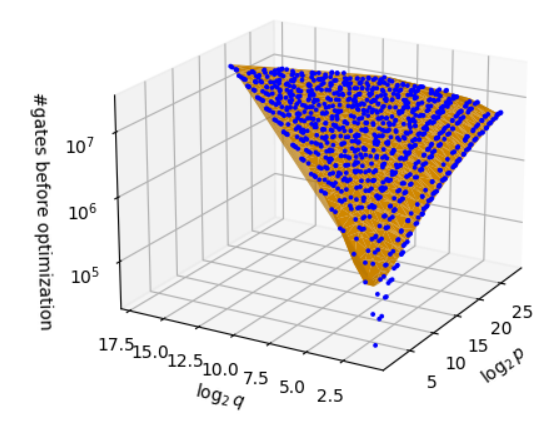
$$= a(\log p)^{3} + (-a + b + c)(\log p)^{2} + (-c + d + e)\log p + (-e + f).$$
(25)

By substituting the parameters (Table 4) into this (25) for each resource and finding the p that matches the results of the Schnorr group in Table 5, we obtain Table 6. Here, it is shown that regardless of optimization, the number of gates, circuit depth, or the number of non-Clifford gates, under Shor's quantum algorithm, a Schnorr group with p = 2048 bits has almost the same cryptographic strength as a safe-prime group with p = 1024 bits. Therefore, it can be inferred that there is a universality independent of the parameters a, b, c, d, e, and f in (23).

Henceforth, we theoretically analyze a more general relational expression for p where the cryptographic strength of the Schnorr group and the safe-prime group becomes equal in quantum computation. According to [2], the combination of bit lengths for p and q in Schnorr groups is (|p|,|q|) = (1024,160), (2048,224), (2048,256), (3072,256),

Table 4:	Parameters of	(23)) obtained	from	the fitting.
----------	---------------	------	------------	------	--------------

	a	b	c	d	e	f
#gates before optimization	2843.058	5260.803	28708.363	-62171.358	-192948.809	459828.645
#gates after optimization	923.891	1720.901	9263.616	-19976.457	-62110.960	148050.262
depth before optimization	1534.728	3178.924	14408.472	-30183.329	-97531.979	228340.308
depth after optimization	694.800	1421.309	6349.034	-13164.850	-42942.880	100263.303
#non-Clifford gates before optimization	1320.030	2444.355	13297.437	-28879.570	-89484.421	213398.262
#non-Clifford gates after optimization	882.216	1647.665	8882.046	-19108.039	-59544.637	141771.038



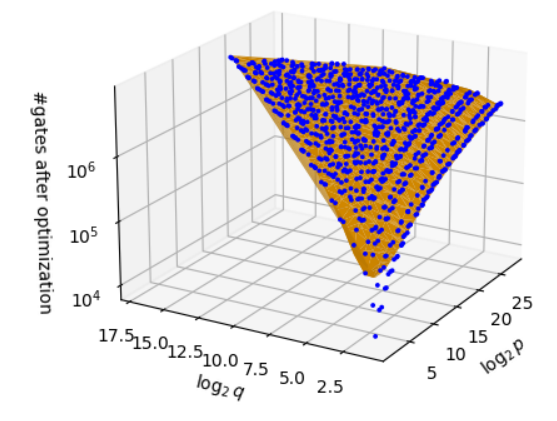


Figure 7: Number of gates before and after optimization. The blue dots represent the results obtained from each experiment, and the orange surface represents (23) using the parameters shown in Table 4.

so approximately

$$\log q = \chi \log p \tag{26}$$

where

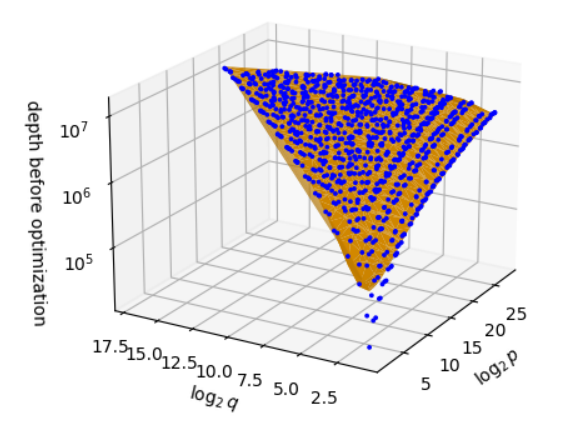
$$\chi \approx 1/10 \tag{27}$$

is expressed. Then, from (23),

$$a(\log p)^2(\chi \log p) + b(\log p)^2 + c(\log p)(\chi \log p) + d\log p + e\chi \log p + f$$
(28)

$$= a\chi(\log p)^{3} + (b + c\chi)(\log p)^{2} + (d + e\chi)\log p + f \quad (29)$$

is obtained. Let $p_{\rm sp}$ be the p of the safe-prime group and $p_{\rm S}$ be the p of the Schnorr group. By transforming the equation



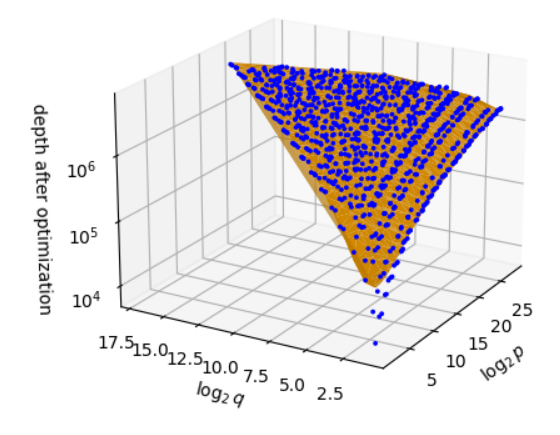


Figure 8: Depth before and after optimization.

that connects (25) and (29) with an equal sign, we get

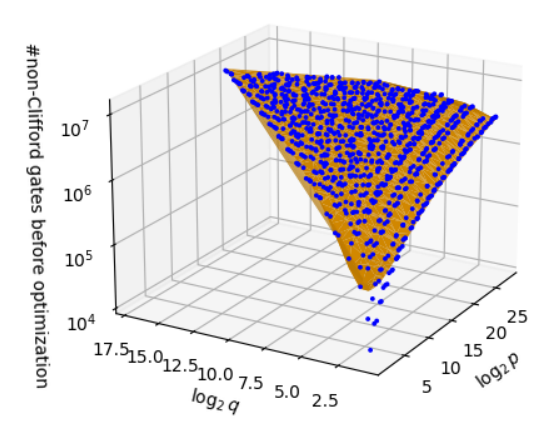
$$a((\log p_{\rm sp})^3 - \chi(\log p_{\rm S})^3) + (-a+b+c)(\log p_{\rm sp})^2 - (b+c\chi)(\log p_{\rm S})^2 + (-c+d+e)\log p_{\rm sp} - (d+e\chi)\log p_{\rm S} - e = 0.$$
(30)

By ignoring the second-order terms of $\log p_{\rm sp}$ and $\log p_{\rm S}$, we have

$$(\log p_{\rm sp})^3 \sim \chi(\log p_{\rm S})^3 \tag{31}$$

$$\log p_{\rm sp} \sim \sqrt[3]{\chi} \log p_{\rm S}. \tag{32}$$

From (27), it is understood that there is a difference of about twice in the bit length of both. In particular, in the Schnorr group with (|p|,|q|) = (2048,256), $\chi = 1/8 = 1/2^3$, so $\log p_{\rm sp} \sim (1/2) \log p_{\rm S}$. This means that under Shor's algorithm, the cryptographic strength of a Schnorr group with p=2048 bits is almost equivalent to that of a safe-prime



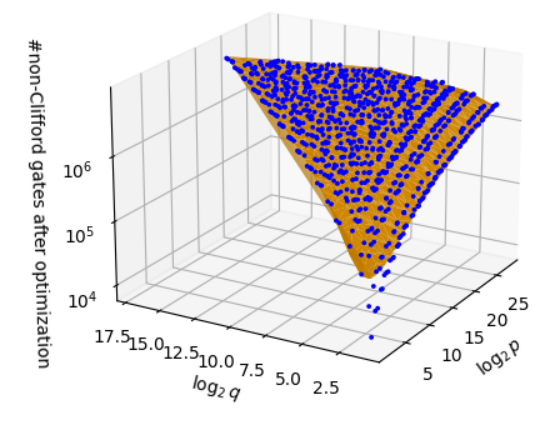


Figure 9: Number of non-Clifford gates before and after optimization.

Table 5: Resource estimation results for safe-prime and Schnorr groups when p is 2048 bits, using R-ADD [28] for modular exponentiation.

modular exponentiation.				
(p , q)	Safe-prime	Schnorr		
(P , q)	(2048, 2047)	(2048, 256)		
#qubits	10241	6659		
#gates	2.46×10^{13}	3.09×10^{12}		
before optimization	2.40 × 10	3.09 × 10		
#gates	7.98×10^{12}	1.00×10^{12}		
after optimization	7.96 × 10			
depth	1.33×10^{13}	1.67×10^{12}		
before optimization	1.55 \ 10			
depth	6.00×10^{12}	7.55×10^{11}		
after optimization	0.00 × 10	7.55 × 10		
#non-Clifford gates	1.14×10^{13}	1.43×10^{12}		
before optimization	1.14 \ 10	1.43×10^{-2}		
#non-Clifford gates	7.62×10^{12}	9.59×10^{11}		
after optimization	1.02 × 10	9.59 × 10		

Table 6: The size of p where the substitution of each parameter into the (25) for the safe-prime group matches the p=2048 bit resource estimation result of the Schnorr group in Table 5.

	p
#gates before optimization	1024.510
#gates after optimization	1024.533
depth before optimization	1024.846
depth after optimization	1024.861
#non-Clifford gates before optimization	1024.515
#non-Clifford gates after optimization	1024.532

with p=1024 bits, reproducing the results shown in Table 6. Therefore, it was shown that the cryptographic strength of the Schnorr group is reduced to about half in terms of the bit length of p in the safe-prime group, regardless of specific parameters.

5 Conclusion

We conducted large-scale quantum simulations of comprehensive combinations of modulo p and order q for Shor's algorithm solving the DLP, which had not been done before. Through 1,860 experiments with all combinations of p and q up to 32 qubits, we obtained a list of actual success probabilities. From this, the correctness of Ekerå's heuristic theoretical analysis [22], which includes periodic fluctuations in success probability due to order q, was demonstrated, and the minimum and maximum values as well as the detailed waveform shape were obtained. Additionally, by extrapolating the circuit scale obtained from experiments with larger combinations of p and q, we estimated the necessary resource values for 2048 bits. From this, we showed that under Shor's quantum algorithm, the Schnorr group has weaker cryptographic strength than the safe-prime group, and furthermore, the cryptographic strength of the Schnorr group experimentally and theoretically decreases to about half the size of p for the safe-prime group.

In the future, we aim to extend this to scenarios assuming quantum error correction as in [10, 11], and to the elliptic curve discrete logarithm problem.

Acknowledgment

The authors are deeply grateful to Martin Ekerå for his various valuable comments, including existing research on the oscillation of success probability.

A 2-controlling qubit trick is optimal in time when time of modular exponentiation > time of measurement

In this section, in relation to Figure 3, we demonstrate that if the time required for modular exponentiation is longer than the measurement time, the computation can be performed in the minimum time with two measurement qubits. Let U be the time required for each unit Mod-MUL of modular exponentiation, and M be the time required for measurement and classical conditional operations. Also, let L be the number of Mod-MUL computations. For Shor's algorithm for factorization, this is twice the number of bits of the composite number, and for Shor's algorithm for DLP, it is given by (11).

Theorem 1. When $U \geq M$, the total time required for the circuit is minimized by

$$LU + M \tag{33}$$

and the minimum number of control qubits to achieve this is 2.

Proof. Since there is only one register for modular exponentiation and L Mod-MULs need to be executed there, the lower bound of the computation time is $L \times U$, and adding the subsequent measurement time M results in (33). Moreover, when there is one control qubit, measurement and classical conditional operations must be executed with only one control qubit each time a Mod-MUL is executed, so the total time is

$$LU + LM = L(U + M). \tag{34}$$

On the other hand, when there are two control qubits, since $U \geq M$, while one control qubit is executing the controlled Mod-MUL, the other control qubit can execute the measurement and classical conditional operations from the previous step, so the total time is given by (33).

B Decision of k such that kcontrolling qubit trick is optimal in time when U < M

In the previous section, we dealt with the case where $U \ge M$, but when U < M, the optimal method differs. Let the

number of control qubits be $k \ll L$. When k=1, the time taken for the entire cicuit is given by (34), whereas for $k \geq 2$, all previous measurement results are required for executing measurements and classically conditioned operations with other control qubits, preventing parallel execution. As a result, it takes a time of

$$U + LM. (35)$$

Therefore, instead of performing the semi-classical inverse quantum Fourier transform one control qubit at a time as traditionally done, we use the so-called half-semi-classical inverse quantum Fourier transform with k qubits as shown in Figure 10. Here, measurements can be executed in parallel with k qubits, so it is expected to be faster when U < M. The time taken for this half-semi-classical inverse quantum Fourier transform can be considered as M when U < M. Thus, the time taken for the entire circuit is

$$LU + \frac{L}{k}M = L\left(U + \frac{1}{k}M\right). \tag{36}$$

Let

$$U = \rho M \tag{37}$$

where $(0 < \rho < 1)$, Then, the following theorem holds.

Theorem 2. When U < M, the value of k for which the total time taken by the circuit using the half-smi-classical inverse quantum Fourier transform is less than when using the semi-classical inverse quantum Fourier transform is given by

$$k > \frac{L}{L + \rho - L\rho}. (38)$$

Proof. By comparing (34) and (36), we have

$$L\left(U + \frac{1}{k}M\right) < U + LM. \tag{39}$$

Substituting (37) and rearranging, we obtain (38).

By combining the previous section with this one, the total time taken by the circuit can be minimized in any case.

C Using another control register as clean qubits in R-ADD

In terms of gate count, a different reduction method from Shor's algorithm for factoring is possible in R-ADD. R-ADD uses 3—controlled NOT and 4—controlled NOT gates, and the number of gates required varies depending on whether the auxiliary bits used for their construction are clean or dirty. Specifically, as shown in [18, 45], a 3—controlled NOT gate requires 3 Toffoli gates when using 1 clean auxiliary qubit, while it requires 4 Toffoli gates when using 1 dirty auxiliary qubit. For a 4—controlled NOT gate, 5 Toffoli gates are needed with 2 clean auxiliary qubits, 6 Toffoli gates with 1 clean and 1 dirty auxiliary qubit, and 8 Toffoli gates

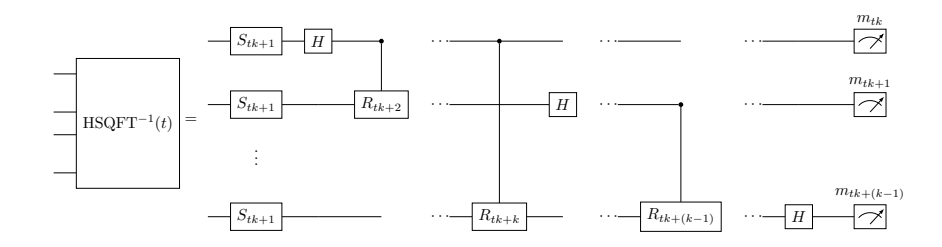


Figure 10: Half-semi-classical inverse quantum Fourier transform. The definitions of R_i and S_j are the same as in Figure 1 and 2.

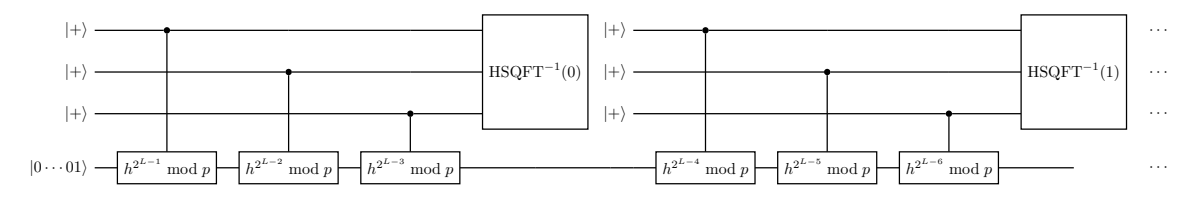


Figure 11: Quantum cicuit for k = 3 using the half-semi-classical inverse quantum Fourier transform (Figure 10).

with 2 dirty auxiliary qubits. In Shor's algorithm for factoring [12,18], the qubits of the control register can be used as clean auxiliary qubits before executing each modular exponentiation module, but one becomes dirty in the second-tolast module, and both become dirty in the last module. On the other hand, in Shor's algorithm for the DLP, there are two control registers, so when performing modular exponentiation from the first control register, the qubits constituting the other control register can be used as clean qubits.

\mathbf{D} DLP Pattern Requiring More Gates Than Other Patterns

In this section, we introduce a group that requires more gates to solve than other DLP groups when the number of qubits is fixed in a quantum computer, although we limit ourselves to cases where neither the semi-classical inverse quantum Fourier transform nor the half-semi-classical inverse quantum Fourier transform is used. This group is referred to as the Same-#qubits group. We seek the combination of p and q that requires the most gates (16) when the number of qubits (13) is fixed. This problem can be generalized with respect to the number of qubits and defined as follows:

Definition 1 (Maximization problem of gate count with fixed qubit number).

$$\alpha x + \beta y - \gamma = 0 \tag{40}$$

subject to the constraint

$$x^m y^n \tag{41}$$

maximization problem. Here, $\alpha, \beta, \gamma, m, n, x, y > 0$.

This can be solved by transforming the constraint (40) to $y = (\gamma - \alpha x)/\beta$ (since y > 0, $x < \gamma/\alpha$) and defining

$$F(x) = x^m y^n = x^m \left(\frac{\gamma - \alpha x}{\beta}\right)^n \tag{42}$$

Table 7: A first derivative test for solving the maximization problem.

x	0		$\frac{\gamma m}{\alpha(m+n)}$		$\frac{\gamma}{\alpha}$
F'(x)	0	+	0	_	
F(x)	0	7	$\frac{\gamma^{m+n}m^mn^n}{\alpha^m\beta^n(m+n)^{m+n}}$	>	0

and using its derivative to write a first derivative test (Table 7). From this result,

$$\lceil \log p \rceil = x = \frac{\gamma m}{\alpha (m+n)}$$

$$\lfloor \log q \rfloor = y = \frac{\gamma n}{\beta (m+n)}$$
(43)

$$\lfloor \log q \rfloor = y = \frac{\gamma n}{\beta (m+n)} \tag{44}$$

is when F(x) is maximized, meaning the most gates are required on a quantum computer.

This can be rewritten as a relational expression between $x = \lceil \log p \rceil$ and $y = \lceil \log q \rceil$:

$$\lceil \log p \rceil = \frac{\beta m}{\alpha n} \lfloor \log q \rfloor. \tag{45}$$

When $p, q \gg 1$, $\lceil \log p \rceil \approx \log p$ and $\lceil \log q \rceil \approx \log q$, so

$$\log p \approx \frac{\beta m}{\alpha n} \log q \tag{46}$$

$$p \approx q^{\frac{\beta m}{\alpha n}} \tag{47}$$

is expressed.

This becomes a simple form when combined with specific calculations of modular exponentiations. For example, using R-ADD, the space complexity is the substitution of (19) into (13), and the time complexity is (20), so $\alpha = 3$, $\beta = 2$, $\gamma = \#$ qubits -4, m = 2, n = 1. Among these, γ does not appear in (47), so

$$p \approx q^{4/3} \tag{48}$$

is obtained. Similarly, in the case of Q-ADD, we have

$$p \approx q^3. \tag{49}$$

Table 8: Resource estimation results for the Schnorr group when p is 2048 bits and the same-#qubits group at the number of qubits of the Schnorr group, using R-ADD [28] for modular exponentiation calculations.

(p , q)	Schnorr	Same-#qubits		
(p , q)	(2048, 256)	(1479, 1109)		
#qubits	6659	6659		
#gates	3.09×10^{12}	6.96×10^{12}		
before optimization	3.03 × 10	0.90 × 10		
#gates	1.00×10^{12}	2.26×10^{12}		
after optimization	1.00 × 10			
depth	1.67×10^{12}	3.75×10^{12}		
before optimization	1.07 × 10	0.10 × 10		
depth	7.55×10^{11}	1.70×10^{12}		
after optimization	7.00 × 10	1.70 × 10		
#non-Clifford gates	1.43×10^{12}	3.23×10^{12}		
before optimization	1.40 \ 10	0.20 / 10		
#non-Clifford gates	9.59×10^{11}	2.16×10^{12}		
after optimization	0.00 × 10	2.10 / 10		

In Simulating Quantum Circuits, p of a safe-prime group was sought to match the time complexity of the Schnorr group, but space complexity was not considered there. By using the same-#qubits group, although limited to cases where the semi-classical inverse quantum Fourier transforms are not used, it is possible to find a combination of p and q with the same space complexity as the Schnorr group and the maximum possible time complexity. The results when using (23) are shown in the Table 8, similar to Table 5. Although not as strong as the safe-prime group in Table 6, it can exceed the resource consumption of the Schnorr group with a smaller p.

In the experiment executing a 36 qubits circuit using Q-ADD, a specific example of p=4093, q=31 was tested, meaning p is 12 bits and q is 5 bits in the same-#qubits group. This values do not seem to follow (49) because $p, q \gg 1$ is not the case, leading to $\lceil \log p \rceil \not\approx \log p$ and $\lfloor \log q \rfloor \not\approx \log q$. The simulation was completed in 30 minutes and is represented in Figures 4, 5, and 12, similar to other samples.

References

- [1] W. Diffie and M. Hellman, "New directions in cryptography," *IEEE Transactions on Information Theory*, vol. 22, no. 6, pp. 644–654, 1976.
- [2] National Institute of Standards and Technology (NIST), "Digital signature standard (dss) federal information processing standards publication 186-4."
- [3] O. Schirokauer, "Discrete logarithms and local units," *Philosophical Transactions of the Royal Society of London. Series A: Physical and Engineering Sciences*, vol. 345, pp. 409 423, 1993.
- [4] E. Barker, L. Chen, A. Roginsky, A. Vassilev, and R. Davis, "Recommendation for pair-wise keyestablishment schemes using discrete logarithm cryptography." NIST SP 800-56A Rev. 3, 2018.

- [5] S. Pohlig and M. Hellman, "An improved algorithm for computing logarithms overgf(p) and its cryptographic significance (corresp.)," *IEEE Transactions on Information Theory*, vol. 24, no. 1, pp. 106–110, 1978.
- [6] D. Shanks, "Class number, a theory of factorization, and genera," vol. 20, pp. 415–440, 1971.
- [7] National Institute of Standards and Technology (NIST), "Digital signature standard (dss) federal information processing standards publication 186-5."
- [8] P. W. Shor, "Algorithms for quantum computation: discrete logarithms and factoring," Proceedings 35th Annual Symposium on Foundations of Computer Science, pp. 124–134, 1994.
- [9] P. W. Shor, "Polynomial-time algorithms for prime factorization and discrete logarithms on a quantum computer," SIAM J. Comput., vol. 26, pp. 1484–1509, 1995.
- [10] C. Gidney and M. Ekerå, "How to factor 2048 bit RSA integers in 8 hours using 20 million noisy qubits," *Quantum*, vol. 5, p. 433, Apr. 2021.
- [11] E. Gouzien and N. Sangouard, "Factoring 2048-bit rsa integers in 177 days with 13 436 qubits and a multimode memory," *Phys. Rev. Lett.*, vol. 127, p. 140503, Sep 2021.
- [12] J. Yamaguchi, M. Yamazaki, A. Tabuchi, T. Honda, T. Izu, and N. Kunihiro, "Estimation of shor's circuit for 2048-bit integers based on quantum simulator." Cryptology ePrint Archive, Paper 2023/092, 2023.
- [13] Y. Akahoshi, K. Maruyama, H. Oshima, S. Sato, and K. Fujii, "Partially fault-tolerant quantum computing architecture with error-corrected clifford gates and space-time efficient analog rotations," *PRX Quantum*, vol. 5, p. 010337, Mar 2024.
- [14] R. Toshio, Y. Akahoshi, J. Fujisaki, H. Oshima, S. Sato, and K. Fujii, "Practical quantum advantage on partially fault-tolerant quantum computer," 2024.
- [15] Y. Akahoshi, R. Toshio, J. Fujisaki, H. Oshima, S. Sato, and K. Fujii, "Compilation of trotter-based time evolution for partially fault-tolerant quantum computing architecture," 2024.
- [16] T. Itogawa, Y. Takada, Y. Hirano, and K. Fujii, "Even more efficient magic state distillation by zero-level distillation," 2024.
- [17] C. Gidney, N. Shutty, and C. Jones, "Magic state cultivation: growing t states as cheap as cnot gates," 2024.
- [18] J. Yamaguchi, M. Yamazaki, A. Tabuchi, T. Honda, T. Izu, and N. Kunihiro, "Experiments and resource analysis of shor's factorization using a quantum simulator," in *Information Security and Cryptology – ICISC* 2023 (H. Seo and S. Kim, eds.), (Singapore), pp. 119– 139, Springer Nature Singapore, 2024.

- [19] M. Ekerå, "Quantum algorithms for computing general discrete logarithms and orders with tradeoffs," *Journal* of Mathematical Cryptology, vol. 15, no. 1, pp. 359–407, 2021.
- [20] M. Ekerå and J. Håstad, "Quantum algorithms for computing short discrete logarithms and factoring rsa integers," in *Post-Quantum Cryptography* (T. Lange and T. Takagi, eds.), (Cham), pp. 347–363, Springer International Publishing, 2017.
- [21] M. Hhan, T. Yamakawa, and A. Yun, "Quantum complexity for discrete logarithms and related problems," in Advances in Cryptology CRYPTO 2024 (L. Reyzin and D. Stebila, eds.), (Cham), pp. 3–36, Springer Nature Switzerland, 2024.
- [22] M. Ekerå, "Revisiting shor's quantum algorithm for computing general discrete logarithms," 2019.
- [23] A. Mandl and U. Egly, "Implementations for shor's algorithm for the dlp." INFORMATIK 2022, 2022.
- [24] Y. Aono, S. Liu, T. Tanaka, S. Uno, R. V. Meter, N. Shinohara, and R. Nojima, "The present and future of discrete logarithm problems on noisy quantum computers," *IEEE Transactions on Quantum Engineering*, vol. 3, pp. 1–21, 2022.
- [25] O. Regev, "An efficient quantum factoring algorithm," 2023.
- [26] M. Ekerå and J. Gärtner, "Extending regev's factoring algorithm to compute discrete logarithms," in *Post-Quantum Cryptography* (M.-J. Saarinen and D. Smith-Tone, eds.), (Cham), pp. 211–242, Springer Nature Switzerland, 2024.
- [27] S. Beauregard, "Circuit for shor's algorithm using 2n+3 qubits," Quantum Info. Comput., vol. 3, p. 175–185, 3 2003.
- [28] V. Vedral, A. Barenco, and A. Ekert, "Quantum networks for elementary arithmetic operations," *Phys. Rev. A*, vol. 54, pp. 147–153, 7 1996.
- [29] R. Rivest and R. Silverman, "Are 'strong' primes needed for RSA." Cryptology ePrint Archive, Paper 2001/007, 2001.
- [30] A. Joux and R. Lercier, "Discrete logarithms in gf(p) 130 digits." an email announcement, June 2005.
- [31] A. Dorofeev, D. Dygin, and D. Matyukhin, "Discrete logarithms in gf(p) 135 digits." an email announcement, Dec. 2006.
- [32] T. Kleinjung, "Discrete logarithms in gf(p) 160 digits." an email announcement, Feb. 2007.
- [33] C. Bouvier, P. Gaudry, L. Imbert, H. Jeljeli, and E. Thomé, "Discrete logarithms in gf(p) 180 digits." an email announcement, June 2014.

- [34] T. Kleinjung, C. Diem, A. K. Lenstra, C. Priplata, and C. Stahlke, "Discrete logarithms in gf(p) 768 bits." an email announcement, June 2016.
- [35] F. Boudot, P. Gaudry, A. Guillevic, N. Heninger, E. Thomé, and P. Zimmermann, "795-bit factoring and discrete logarithms." an email announcement, Dec. 2019.
- [36] F. Boudot, P. Gaudry, A. Guillevic, N. Heninger, E. Thomé, and P. Zimmermann, "Comparing the difficulty of factorization and discrete logarithm: a 240digit experiment." Cryptology ePrint Archive, Paper 2020/697, June 2020.
- [37] F. Boudot, P. Gaudry, A. Guillevic, N. Heninger, E. Thomé, and P. Zimmermann, "Comparing the difficulty of factorization and discrete logarithm: A 240-digit experiment," in Advances in Cryptology – CRYPTO 2020: 40th Annual International Cryptology Conference, CRYPTO 2020, Santa Barbara, CA, USA, August 17–21, 2020, Proceedings, Part II, (Berlin, Heidelberg), p. 62–91, Springer-Verlag, 2020.
- [38] M. A. Nielsen and I. L. Chuang, Quantum Computation and Quantum Information: 10th Anniversary Edition. USA: Cambridge University Press, 10th ed., 2011.
- [39] Y. Suzuki, Y. Kawase, Y. Masumura, Y. Hiraga, M. Nakadai, J. Chen, K. M. Nakanishi, K. Mitarai, R. Imai, S. Tamiya, T. Yamamoto, T. Yan, T. Kawakubo, Y. O. Nakagawa, Y. Ibe, Y. Zhang, H. Yamashita, H. Yoshimura, A. Hayashi, and K. Fujii, "Qulacs: a fast and versatile quantum circuit simulator for research purpose," Quantum, vol. 5, p. 559, Oct. 2021.
- [40] S. Imamura, M. Yamazaki, T. Honda, A. Kasagi, A. Tabuchi, H. Nakao, N. Fukumoto, and K. Nakashima, "mpiqulacs: A distributed quantum computer simulator for a64fx-based cluster systems," 2022.
- [41] N. Kunihiro, "Exact analyses of computational time for factoring in quantum computers," *IEICE Trans. Fundam. Electron. Commun. Comput. Sci.*, vol. 88-A, pp. 105–111, 2005.
- [42] T. G. Draper, "Addition on a quantum computer," 2000.
- [43] P. Virtanen, R. Gommers, T. E. Oliphant, M. Haberland, T. Reddy, D. Cournapeau, E. Burovski, P. Peterson, W. Weckesser, J. Bright, S. J. van der Walt, M. Brett, J. Wilson, K. J. Millman, N. Mayorov, A. R. J. Nelson, E. Jones, R. Kern, E. Larson, C. J. Carey, İ. Polat, Y. Feng, E. W. Moore, J. VanderPlas, D. Laxalde, J. Perktold, R. Cimrman, I. Henriksen, E. A. Quintero, C. R. Harris, A. M. Archibald, A. H. Ribeiro, F. Pedregosa, P. van Mulbregt, and SciPy 1.0 Contributors, "SciPy 1.0: Fundamental Algorithms for Scientific Computing in Python," Nature Methods, vol. 17, pp. 261–272, 2020.

- [44] National Institute of Standards and Technology (NIST), "Digital signature standard (dss) federal information processing standards publication 186-3."
- [45] A. Barenco, C. H. Bennett, R. Cleve, D. P. DiVincenzo, N. Margolus, P. Shor, T. Sleator, J. A. Smolin, and H. Weinfurter, "Elementary gates for quantum computation," *Phys. Rev. A*, vol. 52, pp. 3457–3467, Nov 1995.

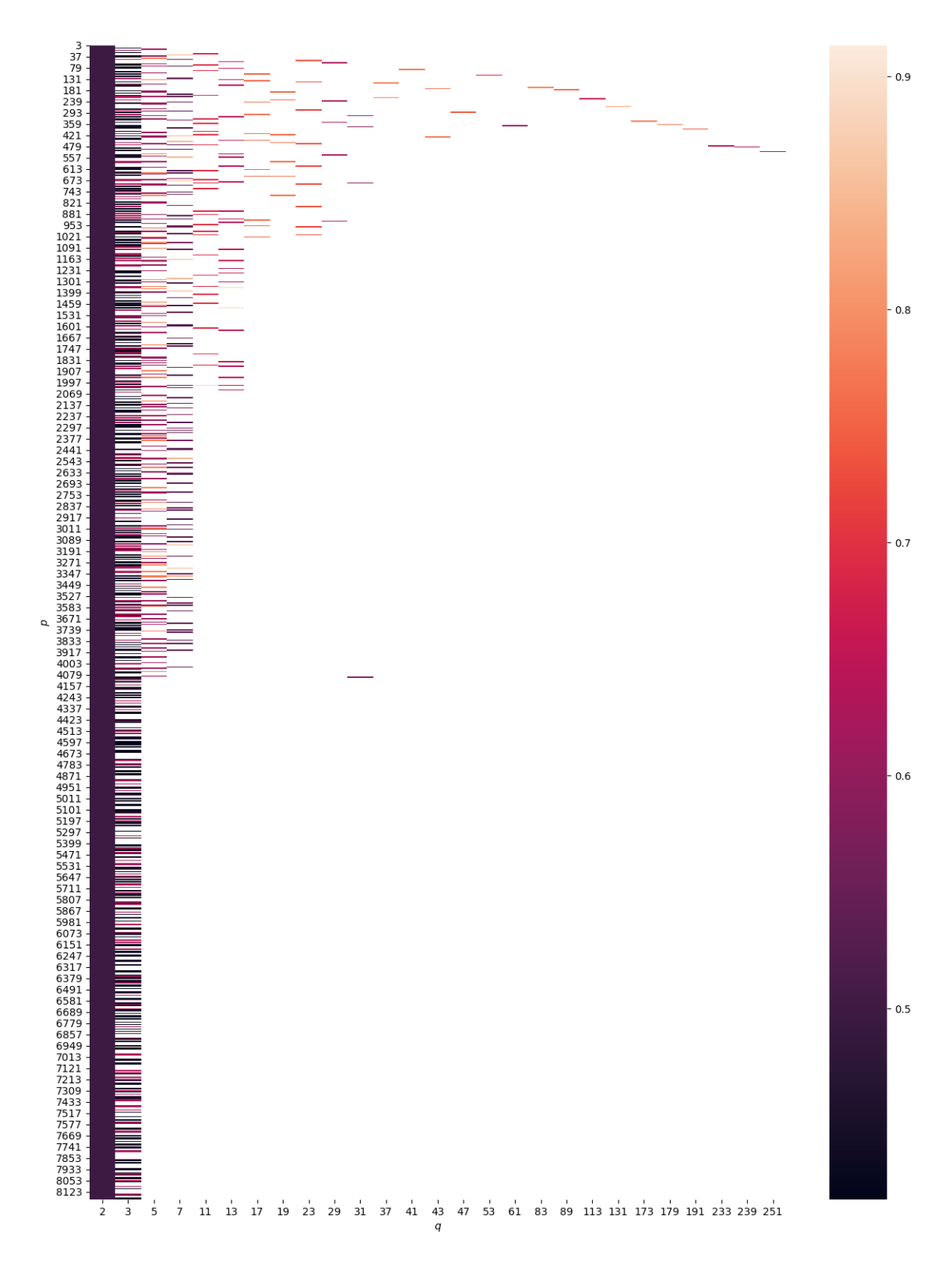


Figure 12: Heatmap of success probabilities for each combination of p and q. Brighter colors indicate success probabilities closer to 1.